ChemPubSoc Europe

DOI: 10.1002/cctc.201800784

CHEMCATCHEM Full Papers

Large Dimensional CeO_2 Nanoflakes by Microwave-Assisted Synthesis: Lamellar Nano-Channels and Surface Oxygen Vacancies Promote Catalytic Activity

Huihui Ding,[a] Jingxia Yang,*[a, b] Shuyi Ma,[a] Nevzat Yigit,[b] Jingli Xu,[a] Günther Rupprechter,[b] and JinJie Wang*[a]

Large nano-structured flakes of CeO_2 (20–80 nm in thickness, up to 5.6 μm in diameter) were synthesized by a combination of microwave (MW), ultraviolet (UV) and ultrasound (US), with or without pressure (P). The CeO_2 structures were systematically examined by XRD, SEM, N_2 sorption, HRTEM, XPS, Raman and H_2-TPR. The synthesized CeO_2 nanoflakes were composed by 3.0–7.5 nm nanoparticles with the (111) surface exposed, and laminated to nanoflakes with 3.42–3.85 nm nano-channels in between. MW-assisting was beneficial to form a higher surface $Ce^{3+}/(Ce^{3+}+Ce^{4+})$ ratio and surface oxygen vacancies during short synthesis procedure. A Raman peak at 480 cm^{-1} correlating with bulk Ce^{3+} was detected. H_2-TPR found MW and MW + P had more surface Ce^{3+} (surface oxygen vacancies). CO oxidation and imine conversion proved that MW + P was the optimum condition to produce highly active CeO_2 nanoflakes. The much better catalytic performance than CeO_2 from solvothermal preparation, due to the larger channel gap (3.85 nm),a higher $Ce^{3+}/(Ce^{3+}+Ce^{4+})$ ratio (32%) and more surface oxygen vacancies on the particles of the organized flake structures.

Introduction

Although CeO_2 has been used widely as catalyst (support) due to its unique and excellent oxygen storage (-release) capacity (OSC), studies of CeO_2 and ceria-based materials are still continuing, with efforts to improve the $Ce^{3+}/(Ce^{3+}+Ce^{4+})$ ratio (shorted as "Ce^{3+} ratio") and specific surface area and thus the catalytic performance for both high temperature reactions (e.g. CO oxidation,[1] NOx reductions.[2] etc.) and low temperature conversions (e.g. imine synthesis,[3] dye degradation[4] and other reactions). Microwave-assisted synthesis is an efficient route towards CeO_2, as it can not only dramatically shorten the reaction time (as compared to conventional solvothermal or sol-gel methods), but also yield products with excellent properties because more defects existed during short microwave-assisted synthesis procedure.[5] It has been reported that microwave-assisted synthesis can produce CeO_2 with smaller particles (size around 3.3–4.0 nm), higher Ce^{3+} ratio, which is more active for methanol oxidation than samples obtained by precipitation.[5a]

[a] H. Ding, Dr. J. Yang, S. Ma, Prof. J. Xu, Dr. J. Wang
College of Chemistry and Chemical Engineering
Shanghai University of Engineering Science
LongTeng Road 333
Shanghai 201620 (P. R. China)
E-mail: yjx09tj@foxmail.com
jxyang@sues.edu.cn
jinjiewang0331@163.com

[b] Dr. J. Yang, N. Yigit, Prof. G. Rupprechter
Institute of Materials Chemistry
Technische Universität Wien
Getreidemarkt 9/BC/01
Vienna 1060 (Austria)

Supporting information for this article is available on the WWW under https://doi.org/10.1002/cctc.201800784

Different morphologies of CeO_2 can also be obtained by microwave-assisted routes, such as nanoparticles,[5b–d] hollow nanospheres,[5e] core-shell structures,[6] nanocubes,[7] nanowires,[7a,8] and small nanoflakes (< 200 nm in diameter).[9] Nanoflake-structured CeO_2 has shown excellent properties in sensors[10] or catalytic applications[11] due to more defects exposed on the surface of layered structure. However, to date there were only few reports about nanoflakes of CeO_2, and most of the sheets had a small size (< 200 nm in diameter)[9–10,12] or were hybrids with other materials.[11b,13] CeO_2 nanoflakes with large dimension and thin layers is still waiting for development, which probably exhibit outstanding properties due to more defects exposing on the particle surface of thin layers and easy transfer of active oxygen atoms (O*) within the organized layer particles. Similar advantages also exhibited in other nanoflake-like catalyst systems.[14] Besides, lamellar channel like structure may be formed in such nanoflake structures, which can be benefit to catalytic performance similar as the honeycomb structure of three-way catalyst.

Microwave-aided synthesis can be carried out in different conditions, such as with or without pressure (pressure in the range of 3–5 atm; equal to microwave assistant solvothermal method). Theoretically, ultraviolet light (UV) and ultrasonic (US) can have effects on CeO_2 too. UV radiation can cause different surface structures of CeO_2 because UV energy can irradiate different form of organic compounds during microwave assisting synthesis, similar to UV induced organic reactions. US application can avoid agglomeration of the products during synthesis. From the economic and scientific view, it is important to figure out how these parameters can influence the CeO_2 structures during microwave assisted synthesis, and how they can further affect the catalytic abilities of CeO_2 materials.

In this study, a series of CeO_2 samples with large nanoflake structures were synthesized by a high-temperature solution

© 2018 Wiley-VCH Verlag GmbH & Co. KGaA, Weinheim

method, assisted by microwave (MW), ultrasonic (US) or ultraviolet light (UV). A solvothermal method was also used to synthesize CeO_2 as a reference. The synthesized CeO_2 nanoflakes were characterized by XRD, SEM, BET, HRTEM, XPS, Raman and H_2-TPR, to figure out the structure and defect distributions. The obtained samples were used as catalysts for CO oxidation and imine synthesis (a kind of important intermediate in biological and pharmaceutical applications) to check the catalytic performances. Finally, relationships between CeO_2 catalytic properties and material structures were proposed.

Results and Discussion

Structure of CeO_2 Synthesized by Microwave

The as-prepared samples were characterized by XRD and crystalline structures were observed. However, the crystalline structures were mixtures as indicated by the change of the relative peak intensities. Previous literature reported that microwave-assisted as-prepared samples had phases like $Ce(HCOO)_3$ (JCPDS No. 49-1245)[15] or $CeCO_3OH$ (JCPDS No. 41-0013),[16] here only part of the peaks belong to $CeCO_3OH$ (Figure 1). The strongest peak at low diffraction angle was probably caused by the ordered lamellar structure, which was self-assembled by organic residues and PVP surfactant, as shown by the following SEM and TEM results. The layer distance was about 1.0 nm based on the diffraction peak 2 theta = 8.801°. After the samples were calcined at 500 °C in the air for 1 h, the organic residues were removed and the typical CeO_2 crystalline phases (JCPDF No: 34-0394) appeared. The crystalline degrees of these samples are different. UV and pressure (P) were benefits to get larger crystalline particles, while US suppressed the particles growth and resulted in larger BET surface area because of ultrasonical dispersion. When the particle sizes are calculated by Scherrer equations based on the strongest peak at 28.5°, the particle sizes were in the range of 3.0 nm–7.5 nm.

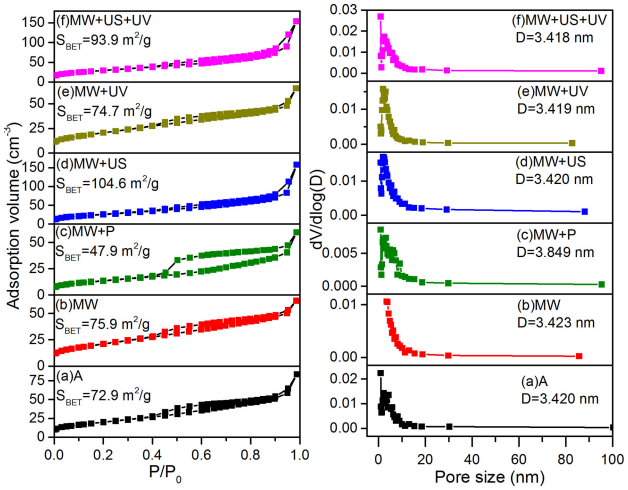

Figure 2. N_2 sorption isotherm (left) and pore size distribution (right) of CeO_2 prepared under different conditions and calcined at 500 °C in air for 1 h.

The calcined samples were further characterized by N_2 sorption isotherms (Figure 2 left) and the pore size distribution was calculated from the desorption branch of the isotherm (Figure 2 right). The hysteresis loops of N_2 sorption isotherm belong to H3 or H4 according to IUPAC classification,[16] associated with plate-like particles giving rise to slit-shaped pores. This is consistent with the samples morphologies observed by SEM and TEM. The MW + US sample possessed the largest specific surface area, S_{BET} 104.6 m^2/g, while sample MW + P had the lowest S_{BET} of 47.9 m^2/g. The ultrasound reduced the crystalline particles' size and increased the surface area. The widest pore size distributions were in the range of 0 ~ 10 nm, and the average pore size was around 3.42 nm, except for sample MW + P, having a little larger average pore size of 3.85 nm. This can be attributed to the PVP structure directing.

The SEM morphologies of the calcined CeO_2 are shown in Figure 3 (a)–(f). All samples exhibited a flake structure with thickness of 20–80 nm, while the diameter can reach to more

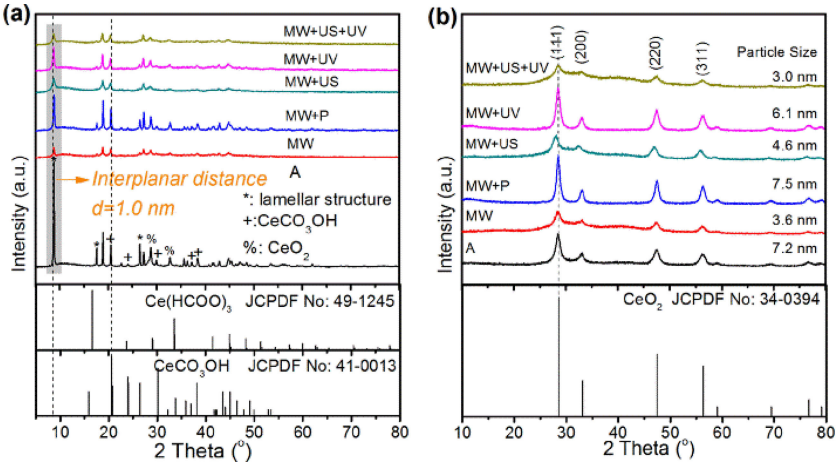

Figure 1. XRD of CeO_2 prepared using different conditions, (a) as-prepared, (b) calcined at 500 °C in air for 1 h. The particle sizes are calculated by Scherrer equations based on the strongest peak at 28.5°.

© 2018 Wiley-VCH Verlag GmbH & Co. KGaA, Weinheim

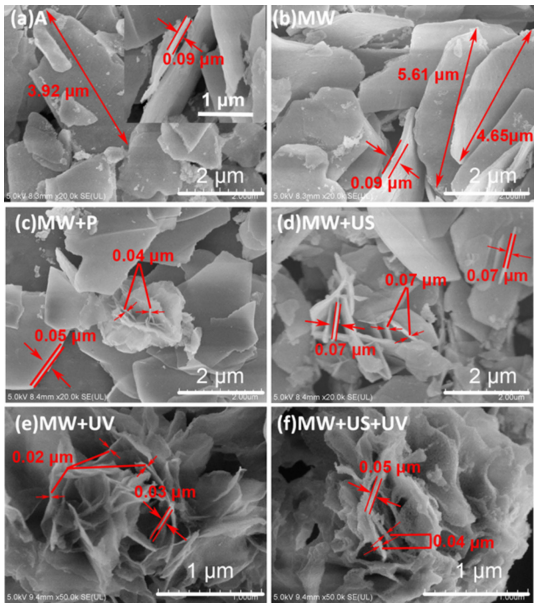

Figure 3. SEM morphologies of CeO_2 prepared using different conditions and calcined at 500 °C in air for 1 h.

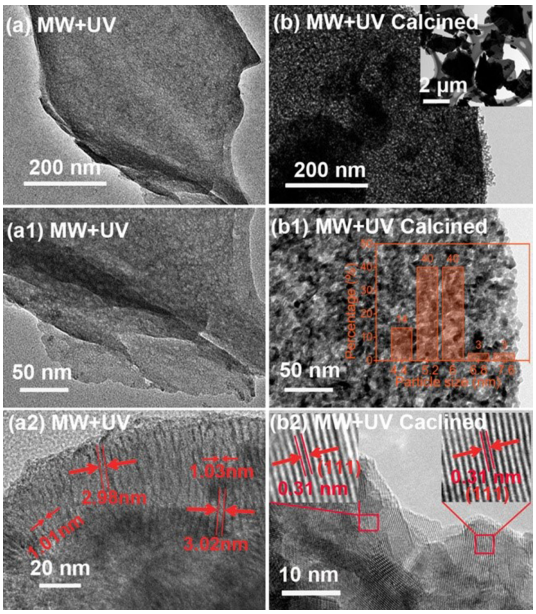

Figure 4. TEM and HRTEM of CeO_2 prepared by MW + UV. (a-a2) are as-prepared CeO_2, (b-b2) are samples further calcined at 500 °C in air for 1 h.

than 5 μm. When ultraviolet light was used as assistance (MW + UV, MW + UV + US), the layer became thinner, which may be related to the chemical changes caused by UV light. Similar thin layers can also be observed in MW + P sample. This agrees with the hysteresis loops of N_2 sorption isotherms, resulting in slit-shaped pores. Flake-like CeO_2 structures were reported before, but the flake sizes were much smaller (< 200 nm in diameter) than those in this study.[9,17]

Sample MW + UV was further characterized by TEM because of the thinner layer structure. It was found that the plate structure was composed of very thin layers before calcination (Figure 4 (a-a1). In some areas fence like structure was observed (Figure 4 (a2)), probably corresponding to the cross-section of the layer structure. These layers may yield the strong XRD diffraction at 2 theta = 8.801°. The thickness of one thin layer and distances in between were about 1 and 3 nm, respectively. This is almost consistent with 3.42 nm pore size of slit-shaped pores in N_2 adsorption results. After calcinations, the large layer structure was still existed (b), but small crystalline particles with a size of about 5–6 nm were observed (b1), in which the lattice distance was 0.31 nm (b2), corresponding to (111) facet.

The structure sketches were proposed in Figure 5. According to XRD, SEM and TEM results, the as-prepared nanoflakes were composed by $CeCO_3OH$, CeO_2 and other unknown crystalline materials. These materials were organized in 1 nm thin layers, and laminated to thicker nanoflakes with 3 nm gap in between from TEM (Figure 5 (a)). After calcination, the Ce containing layers were decomposed and transformed to crystalline CeO_2 (3.0–7.5 nm in diameter), the lamellar structure preserved, and the gap in between was about 3.42–3.85 nm from pore size distribution of N_2 sorption (Figure 5 (b)). These gaps can serve as reaction channels of catalytic reactions to improve the CeO_2 performance, which is similar to the honeycomb channels of three-way catalyst.

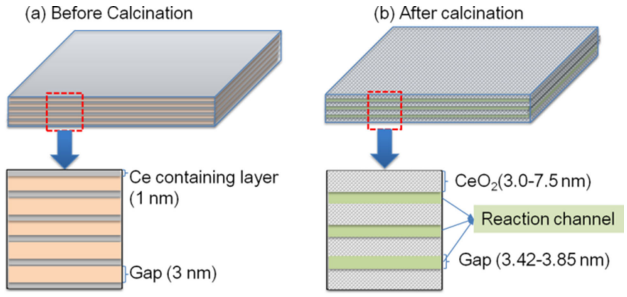

Figure 5. Structure sketch of CeO_2 nanoflakes before and after calcination.

XP spectra were used to characterize the valence states of the calcined CeO_2 (Figure 6) and the Ce 3d regions were examined. Normally, the Ce 3d region is formed by five doublets (V denotes Ce 3d5/2, U denotes Ce 3d3/2). V^0, V′, U^0, U′ belong to Ce^{3+} species, while V, V″, V‴, U, U″ and U‴ belong to Ce^{4+} species. To determine the Ce^{3+} ratio, the peak areas of the U^0 (V^0) and U′ (V′) peaks were related to the area of the entire Ce 3d region.[1c] The autoclaved CeO_2 (A) exhibited a Ce^{3+} ratio of 22.5%, lower than the value of most microwave assisted samples (except MW sample). For the microwave assisted samples, the highest Ce^{3+} ratio of 32.5% belonged to MW + P, while sample MW showed the lowest Ce^{3+} value of 21.4%. The ultrasound assistance produced a higher Ce^{3+} ratio (MW + US: 28.9%) than the UV aided sample (MW + UV: 23.6%). The Ce^{3+} ratio of MW + US + UV was 27.7%, a bit lower than that of MW + US, which may be due to UV irradiation. The higher Ce^{3+} ratio of microwave-aided samples can be attributed to the shorter synthesizing time, causing more defects in the samples.[5]

Raman was used to detect the defects in the synthesized CeO_2, as shown in Figure 7. Unlike most of the literature that

© 2018 Wiley-VCH Verlag GmbH & Co. KGaA, Weinheim

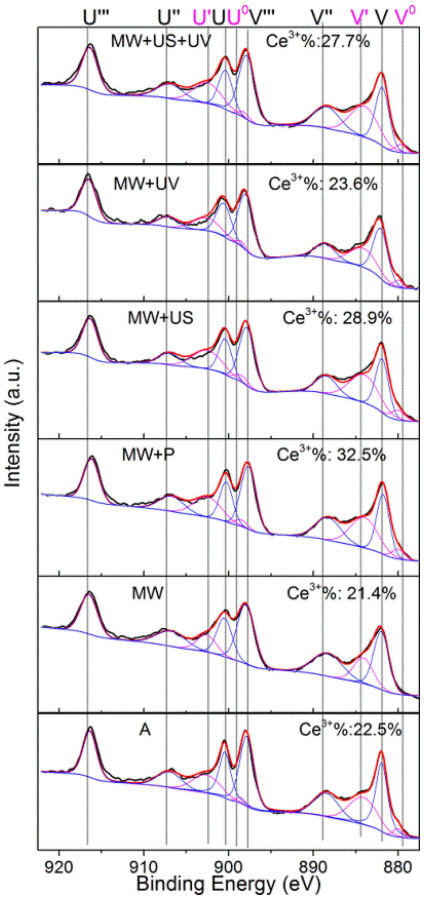

Figure 6. The region of Ce 3d XP spectra of CeO_2 prepared using different conditions and calcined at 500 °C in air for 1 h.

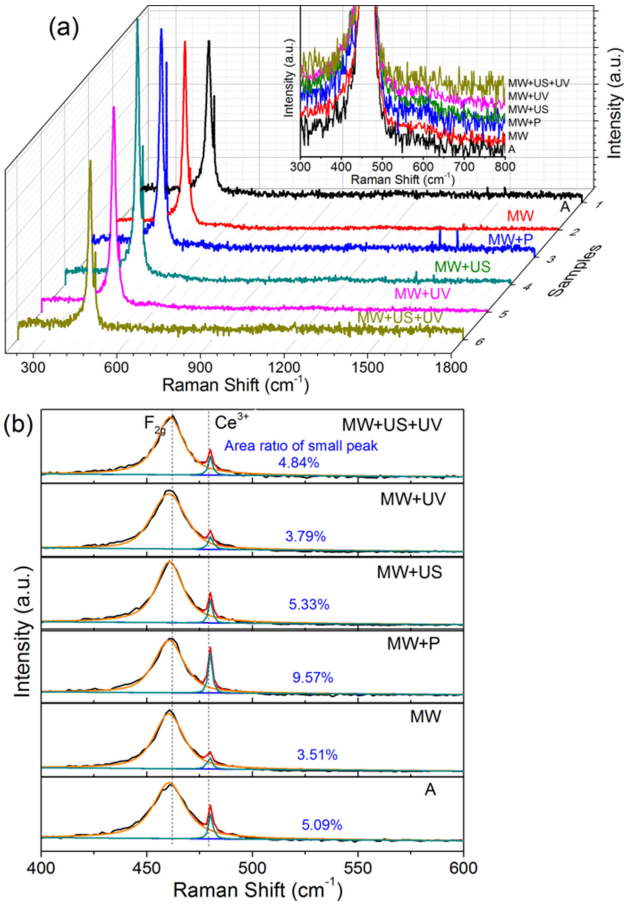

Figure 7. Raman spectra of CeO_2 prepared using different conditions and calcined at 500 °C in air for 1 h. (a) Raman spectra in the region of 200–1800 cm^{-1}. (b) Peak fitting in the region of 400–600 cm^{-1}.

the oxygen defects caused a shoulder peak at 500–600 cm^{-1} in Raman spectra,[18] all the samples we synthesized had a sharp peak at 480 cm^{-1} besides the peak at 460 cm^{-1} (lattice oxygen motion (F_{2g} mode)) and the shoulder peak at 500–600 cm^{-1} (defects). Although no literature discussed this peak for experimental data, the peaks at 480 cm^{-1} were also observed in some nanorods researches (e.g. Ref. [19] Figure 10, Ref. [20] Figure 7). When the 480 cm^{-1} sharp peak appeared, the intensity of shoulder peak became dramatically weak.[19–20] Similar situation can also be found in this research, all shoulder peaks were not very large and it's very difficult to evaluate the difference of samples defects basing on this.

While CeO_2 Raman spectra was calculated by a Density Functional Theory(DFT),[21] the CeO_{2-x} displayed signature vibrational bands in the 480–600 cm^{-1} region associated with the presence of oxygen defects and reduced Ce^{3+} ions. They found that bulk CeO_{2-x} Raman bands arising from Ce^{3+} in direct proximity to the oxygen defect characterized by a calculated band at 500 cm^{-1}, and those originating from Ce^{3+} located in the second coordination sphere of the oxygen vacancy, giving rise to a sharp band at 480 cm^{-1} (Table 4 & Figure 6 in Ref. [21]). In this research, the nanoflakes were composed by small CeO_2 particles of 3.0–7.5 nm, which was comparable to the $Ce_{32}O_{64}$ cell model (ca. 2–3 nm) in Ref.[21] Thus, the sharp peak at 480 cm^{-1} here can be recognized as the response of Ce^{3+} which located in the second coordination sphere of the oxygen vacancy in the CeO_{2-x} bulk. After peak fitting, the area ratios of peak 480 cm^{-1} were calculated and the sequence is as follows: MW + P (9.57 %) > MW + US (5.33 %) > A (5.09 %) > MW + US + UV (4.84 %) > MW + UV (3.79 %) > MW (3.51 %).

H_2-TPR profiles were shown in Figure 8 in order to detect the relative amount of surface oxygen vacancies, because surface oxygen vacancies have been proved very important both in CO oxidation and imine conversions.[3a,e,f] Two obvious regions were shown at around 460 °C (region I) and 730 °C (region II) (Figure 8(a)), corresponding to surface and bulk oxygen respectively.[22] H_2 consumption amount were marked in each sample curve. Except sample MW + UV and MW + US + UV, sample MW + P exhibited the most H_2 consumption amount (10.32 cm^3/g) while sample A cost the least H_2 (7.89 cm^3/g). Sample MW + UV and MW + US + UV showed higher H_2 consumption amount (about 11.20 cm^3/g), which may be caused by the thinner layer and more oxygen on the surface (see Figure 3). The increase of Ce^{3+} or oxygen vacancies on the surface caused the shift of starting point to lower temperature.[19] The starting points of MW + UV was 325 °C while the temperature of sample MW and MW + P shifted to 250 °C, indicating the latter two has more surface Ce^{3+} or surface

© 2018 Wiley-VCH Verlag GmbH & Co. KGaA, Weinheim

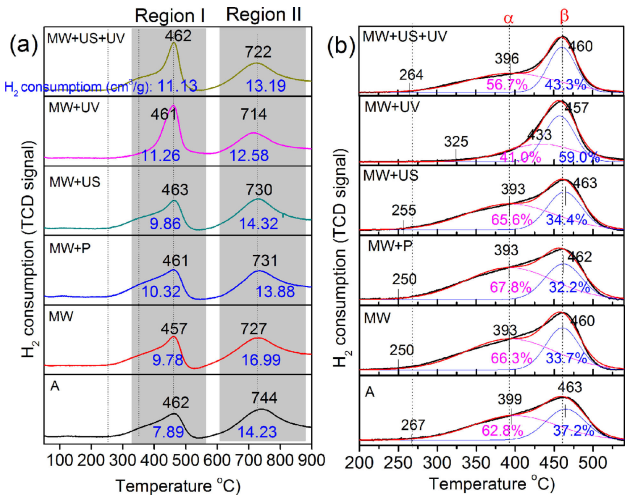

Figure 8. H_2-TPR of CeO_2 prepared using different conditions and calcined at 500 °C in air for 1 h. (a) Full spectra from 50–900 °C; (b) Peak fitting of surface oxygen at 460 °C.

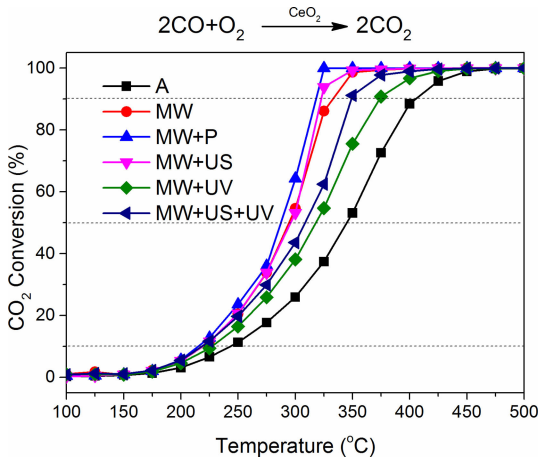

Figure 9. CO oxidation (5 vol% CO in 50 mL/min flow) at different temperatures for CeO_2 samples (20 mg).

oxygen vacancies, and these two also showed good catalytic activity in the following catalytic reactions. Region I can be separated into two peaks at 390 °C (α) and 460 °C (β) (Figure 8(b)), and the former one corresponded to active oxygen (Ce^{3+}–O–Ce^{4+}) which had close relationship with surface Ce^{3+} and surface oxygen defects.[23] The H_2 consumption amounts of the first fitting peak α were calculated basing on the area ratio: MW + P (7.01 cm^3/g) > MW (6.48 cm^3/g) ≈ MW + US (6.47 cm^3/g) > MW + UV + US (6.31 cm^3/g) > A (4.96 cm^3/g) > MW + UV (4.62 cm^3/g), suggesting MW + P possessed the most Ce^{3+} (oxygen vacancies) on the surface, while MW + UV had the least surface Ce^{3+} amount (surface oxygen vacancies). It should be pointed out that sample MW had the lowest Ce^{3+} ratio from XPS and Raman spectra, but the H_2 consumption of peak α of sample MW was much more than sample A. This indicated that the sample MW had more oxygen vacancies on the top surface, resulting in the following good catalytic performances.

Detection of Catalytic Activity

CO oxidation was used to test the catalytic activities of the synthesized samples (Figure 9). The ignition temperature ($T_{10\%}$, the reaction temperature required for 10% CO conversion), and the light-off temperature $T_{90\%}$ (the temperature at which 90% conversion of CO is achieved) were checked, as listed in Table 1. The best sample for CO oxidation was MW + P, with $T_{10\%}$ = 216 °C and $T_{90\%}$ = 318 °C, while the worst performance was due to sample A ($T_{10\%}$ = 243 °C, $T_{90\%}$ = 405 °C). The catalytic activity of the least active sample A is comparable with our previously reported CeO_2 sample CeB/AO/F127-STE ($T_{10\%}$ = 253 °C, $T_{90\%}$ = 398 °C, S_{BET} = 277 m^2/g),[1c] indicating sample MW + P had a much higher catalytic activity. The sequence of $T_{10\%}$ is the same as that of $T_{90\%}$: MW + P (216 °C, 318 °C) < MW + US (220 °C, 322 °C) ≤ MW (220 °C, 333 °C) < MW + US + UV (224 °C, 349 °C) < MW + UV (227 °C, 373 °C) < A (243 °C, 405 °C).

The reaction rates at 250 °C normalized per gram ($r_{250°C}$) and per unit surface area ($R_{250°C}$) are calculated to enable the comparison of the catalytic activity of the different samples using the conversions below 20%, as listed in Table 1. The least

Table 1. Summary of CO oxidation results by using different CeO_2 as catalysts.

Sample	$T_{10\%}$ [a] [°C]	$T_{90\%}$ [b] [°C]	$r_{250°C}$ [c] [mol·s·g]	$R_{250°C}$ [a] [mol/s·m^2]	Condition of CO oxidation reaction
A	243	405	9.08×10^{-6}	1.24×10^{-7}	50 mL/min (5 vol% CO), 0.02 g catalyst
MW	220	333	1.64×10^{-5}	2.16×10^{-7}	
MW + P	216	318	1.90×10^{-5}	3.97×10^{-7}	
MW + US	220	322	1.65×10^{-5}	1.57×10^{-7}	
MW + UV	227	373	1.32×10^{-5}	1.47×10^{-7}	
MW + US + UV	224	349	1.58×10^{-5}	1.69×10^{-7}	
CeB/AO/F127-STE[1c]	253	398	6.42×10^{-6}	2.32×10^{-8}	
CeO2-180[24c]	/	/	5.15×10^{-7}	4.29×10^{-9}	160 mL/min (0.4vol % CO), 0.20 g catalyst (S_{BET} = 120 m^2/g)
CeO2[24a]	/	/	6.44×10^{-6}	2.08×10^{-7}	40 mL/min (1 vol% CO), 0.02 g catalyst (S_{BET} = 31 m^2/g)
CeO2-500[19]	/	320 ($T_{50\%}$)	8.37×10^{-7}	1.12×10^{-8}	30 mL/min (1 vol% CO), 0.03 g catalyst (S_{BET} = 74.5 m^2/g)
CeO2(CeCu0)[24b]		380 ($T_{50\%}$)	1.03×10^{-6}	5.10×10^{-9}	80 mL/min (1 vol% CO), 0.50 g catalyst (S_{BET} = 202 m^2/g)

[a] Reaction temperature for 10% CO conversion; [b] reaction temperature for 90% CO conversion; [c] reaction rate (mol/s g) of CO oxidation at 250 °C per gram, by using the converted mole amount of CO at 250 °C and normalized it to per gram; [d] normalized specific reaction rates (mol/s·m^2) of CO oxidation on a unit surface area at 250 °C, by using the converted mole amount of CO at 250 °C and normalized it to per specific area.

© 2018 Wiley-VCH Verlag GmbH & Co. KGaA, Weinheim

active sample A is with $r_{250°C} = 9.08 \times 10^{-6}$ mol/s·g and $R_{250°C} = 1.24 \times 10^{-7}$ mol/s·m^2, nevertheless higher than the values (6.42×10^{-6} mol/s·g, 2.32×10^{-8} mol/s·m^2) of the best sample CeB/AO/F127-STE we reported before[1c] and other CO oxidation rates.[19,24] The best sample MW+P has an even better catalytic activity, with $r_{250°C} = 1.90 \times 10^{-5}$ mol/s·g and $R_{250°C} = 3.97 \times 10^{-7}$ mol/s·m^2. The $r_{250°C}$ of MW+P was twice than that of sample A, and about 3 times as the value of sample CeB/AO/F127-STE, while $R_{250°C}$ of MW+P was about 16 times higher of sample CeB/AO/F127-STE. The improved catalytic performance of MW-assisting CeO_2 can be contributed to high Ce^{3+} ratio and the organized lamellar channels, although the surface areas are low.

Imine conversion was also tested by using different CeO_2 catalysts (Figure 10), as a model of low temperature catalyst. It has been reported earlier that CeO_2 can be used as an easily separable catalyst for imine synthesis at low temperature (< 100 °C)[5e] and oxygen vacancies played an important role during this reaction (Figure 10 (b)). The order of imine conversion is MW+P (9.52 mmol g^{-1} h^{-1}) > MW (9.13 mmol g^{-1} h^{-1}) > MW+US (7.05 mmol g^{-1} h^{-1}) > MW+US+UV (6.31 mmol g^{-1} h^{-1}) > A (4.87 mmol g^{-1} h^{-1}) > MW+UV (2.84 mmol g^{-1} h^{-1}). This is consistent with the ranking of surface active oxygen in H_2-TPR fitted peak α (Figure 8 (b)). The best imine conversion rate (9.52 mmol g^{-1} h^{-1}) appeared for the system with MW+P as catalyst (higher than the reported 0.46 mmol g^{-1}h^{-1} of sample at 30 °C in Ref. [16] and 4.9 mmol g^{-1}h^{-1} of sample at 50 °C in Ref. [3e]), while the lowest one (2.84 mmol g^{-1} h^{-1}) belonged to sample MW+UV. This generally fits to the rank of the CO oxidation, except MW+UV and A. As the imine conversion worked at 50 °C, the Ce^{3+} migration was not as fast as that at high temperature of CO oxidation (> 200 °C), which may contribute to the inverse performance of MW+UV and A during CO oxidation (> 200 °C). Similar situation can be observed in Fenton-like dye degradation (Figure S4).

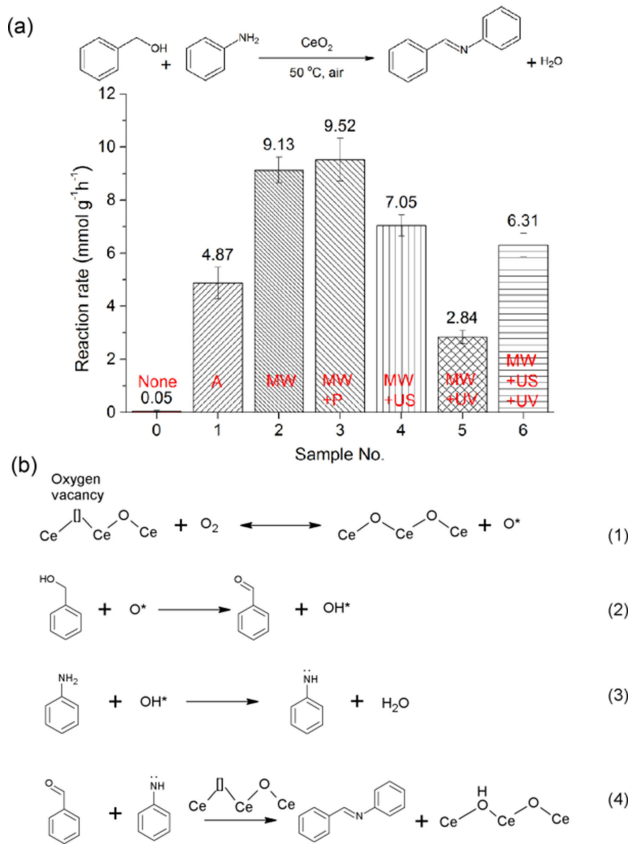

Figure 10. (a) Imine conversion rate (per catalyst amount per hour) by using different CeO_2 (50 mg); all values were calculated for conversion below 20%. The experiments were repeated for 3 times, and the average conversion values were given with error bars. (b) Reaction mechanism of imine conversion by using CeO_2 as catalyst (taken from authors' previous work [3e]).

Parameters Influencing Catalytic Activity

As the previous reaction rates were calculated based on the initial conversion values (lower than 20%) for both CO oxidation and imine conversion, and the lamellar gaps of the CeO_2 flakes were almost the same (3.42 nm) except sample MW+P (3.85 nm), the two catalytic reactions can be recognized as chemical control processing with negligible mass transportation difference. Thus, it's important to figure out that which property of the sample has close relationship with the active sites. Besides the benefit of lamellar reaction channel structure of CeO_2 nanoflakes, the intrinsic properties of CeO_2 nanoparticles can also influence the catalytic ability. Figure 11 shows the parameters influencing the catalytic activity. Depending on the reaction temperature, CO oxidation (high temperature reaction) and imine conversion (low temperature reaction) were chosen as two models. Basically, $Ce^{3+}/(Ce^{3+}+Ce^{4+})$ ratio had close relationship with the catalytic performance of CeO_2 nanoflake except sample MW (Figure 11 (a1) & (b1)). MW showed good catalytic performance although the $Ce^{3+}/(Ce^{3+}+Ce^{4+})$ ratio was the worst one during all samples. Nevertheless, from TPR results, the surface oxygen vacancies of sample MW was more than the others, indicating more Ce^{3+} and more oxygen vacancies stayed on the top surface layer, rather than on sub-surface layers. This compensated the inferior total Ce^{3+} amount, as reported by other literatures.[3e,25] Here, the area ratios of 480 cm^{-1} peak in Raman spectra were also displayed (Figure 11 (a2 & b2)), and the rank was consistent with Ce^{3+} ratio calculated by XPS Ce 3d fitting results, proving that it was caused by Ce^{3+}. When H_2 consumption of H_2-TPR was concerned, the reaction rate of both catalytic reactions fitted quite good with the H_2 consumption amount of peak α (Figure 11 (a4) & (b4)), rather than the H_2 consumption amount of region I (Figure 11 (a3) & (b3)), indicating surface Ce^{3+} amount (surface oxygen vacancies) governed the catalytic activities of CeO_2 nanoflakes, and sample MW had more surface oxygen vacancies. However, the surface area showed no close relationship with the catalytic performance of CeO_2 nanoflakes, which may be because channel gaps were similar (3.4 nm) and the differences of surface areas were not large enough during these nanoflake samples (48–105 m^2/g) (Figure 11 (a5) & (b5)). The only exception was MW+P, with the channel gap of

© 2018 Wiley-VCH Verlag GmbH & Co. KGaA, Weinheim

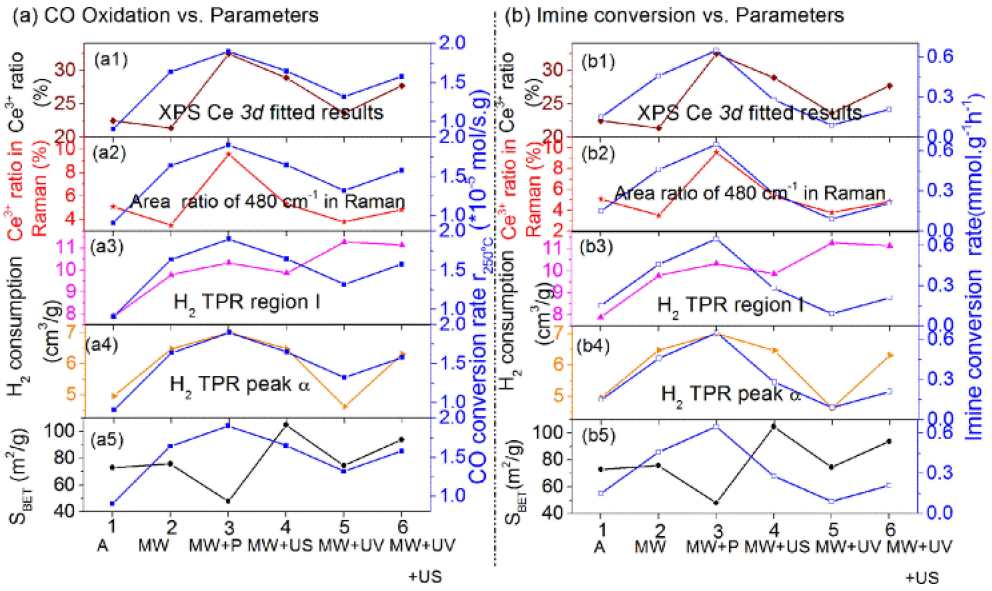

Figure 11. Correlation of catalytic activity with different parameters. (a) CO oxidation rate vs. parameters, (b) imine conversion rate vs. parameters.

3.8 nm. The larger gap allowed more reactant into the channel, beneficial to the catalytic performance.

From the above analysis, it can be seen clearly that the relative amount of surface oxygen vacancies (surface Ce^{3+}) governed the catalytic activity of CeO_2 nanoflakes, rather than the surface area and the bulk oxygen vacancies (bulk Ce^{3+}), as sketched in Figure 12. Generally, the total Ce^{3+} ratio had close

Figure 12. Mechanism sketch of CeO_2 nanoflakes as catalyst for CO oxidation and imine synthesis.

relationship with the amount of surface oxygen vacancies (eg. sample MW+P, MW+US), but sample MW existed as an exception. It had the lowest Ce^{3+} ratio (21%), but most of them stayed on the surface, resulting in high catalytic performance in both CO oxidation and imine synthesis. Sample MW+P exhibited the highest catalytic activity due to abundant Ce^{3+} in both surface and bulk lattices (highest Ce^{3+} ratio: 32%). The nano-layer gap of CeO_2 nanoflakes can serve as reaction channel, in which the reactant had more chance to get access to active oxygen atom during going through the channel, than just on the surface. Thus, the lager channel gap of sample MW+P (3.85 nm) was also better than smaller channel gap (3.42 nm) of other samples, because larger channel gap can allow reactant getting into the flakes much easier.

Conclusions

A series of CeO_2 samples with nanoflake structure (20–80 nm in thickness, up to 5.6 μm in diameter) were synthesized by the assistance of MW, UV and US combinations, with or without applied pressure (P). The CeO_2 structures were systematically characterized by XRD, SEM, HRTEM, N_2 sorption, XPS, Raman and H_2-TPR. The synthesized nanoflakes possessed lamellar channels of 3.42–3.85 nm. Microwave assistance was beneficial to form a higher surface $Ce^{3+}/(Ce^{3+}+Ce^{4+})$ ratio and surface oxygen vacancies. Raman spectra showed a peak at 480 cm^{-1}, corresponding to Ce^{3+} in the bulk, and the fitted value sequence was almost consistent with the $Ce^{3+}/(Ce^{3+}+Ce^{4+})$ ratio of XPS spectra. The results indicated that sample MW+P exhibited the largest channel gap, the highest $Ce^{3+}/(Ce^{3+}+Ce^{4+})$ ratio (32%) and the most surface Ce^{3+} (H_2 consumption of peak α 7.01 cm^3/g), while the MW sample possessed the lowest $Ce^{3+}/(Ce^{3+}+Ce^{4+})$ ratio (21%) but more surface Ce^{3+} (H_2 consumption of peak α 6.48 cm^3/g). CO oxidation and imine conversion proved that MW+P was the optimum condition to produce high quality CeO_2 nanoflakes catalysts bearing abundant defects on the surface, which exhibited much higher catalytic activity than CeO_2 prepared by solvothermal method. The performance of CeO_2 nanoflakes was more dependent on the laminal channel gap, $Ce^{3+}/(Ce^{3+}+Ce^{4+})$ ratio and especially surface oxygen vacancies, rather thanjust the specific surface area.

Experimental Section

Cerium (III) nitrate hexahydrate ($Ce(NO_3)_3 \cdot 6H_2O$), urea, polyvinylpyrrolidone (PVP, K10–14), are used as starting materials with ethylene glycol (EG) being used as solvent. All materials were AR grade and used as received. The microwave, ultrasonic and ultraviolet light were used to assist the synthesis of CeO_2.

© 2018 Wiley-VCH Verlag GmbH & Co. KGaA, Weinheim

Preparation of CeO_2

For all synthesis routes, the solution content and the reaction temperature were the same, and as well as the preparation procedure. First, 5 mmol $Ce(NO_3)_3 \cdot 6H_2O$ and 0.5 g PVP were dissolved in 20 mL EG, named as solution A; 7.5 mmol urea and 0.5 g PVP were dissolved in 15 mL EG to form solution B. Then solution B was slowly added into solution A, and further stirred for 20 min to form a stable and uniform reaction solution.

For CeO_2 synthesis, the microwave assisted reactions were carried on a Multifunctional Microwave Synthesis & Extraction Workstation, Model Uwave-2000 from SINEO Microwave Chemistry Technology (China) Co., Ltd. This equipment can combine microwave, ultrasonic and ultraviolet light together during the synthesis. It can also be used to perform reactions under pressure (3 atm) with microwave irradiation, equal to microwave assisted solvothermal reaction. The power of microwave can be adjusted in the range of 0–1000 W by variable frequency. The ultrasonic powder was 300 W. The wavelength of ultraviolet light was 365 nm and the powder was 300 W. For all synthesis with microwave assistance, the heating programs were the same. The temperature was risen to 180 °C at 15 °C/min ramping rate, and then kept at 180 °C for 10 min. The synthesis conditions for all samples are summarized in Table 2. For the synthesis without pressure, the reaction solution was poured into a four-necked quartz flask, which was connected with a condenser to prevent solvent evaporation at high temperature.

After the reaction processing, the container was cooled to below 50 °C before the suspensions were transferred for separation. All synthesized samples were centrifuged and washed by ethanol at least 3 times. The final white or yellowish precipitates were collected and dried in vacuum at 65 °C overnight, named as-prepared samples. Part of the as-prepared samples were further calcined at 500 °C (2 °C/min ramping rate) for 1 h in air to remove surface organic residues.

Characterization of CeO_2 Catalytic Activity

Before the CO oxidation catalytic test, all calcined CeO_2 samples were treated at 300 °C in air for at least 30 min to activate the surface (heating ramping rate was 10 °C/min) in quartz reactor in synthetic air. For imine synthesis, the activation took place in Al_2O_3 crucible.

CeO_2 as Catalyst for CO Oxidation

CO oxidation was performed in a continuous-flow fixed-bed quartz reactor under atmospheric pressure. 20 mg CeO_2 was loaded into the reactor and pretreated with synthetic air (30 mL/min) at 300 °C for 30 min (heating rate 10 °C/min). Then the sample was cooled to 30 °C in flowing synthetic air, and a mixture of 5 vol% CO, 10 vol% O_2 and 85 vol% He (total flow 50 mL/min) was introduced. The system was then heated to 500 °C with a ramp of 5 °C min^{-1}. The concentrations of CO and CO_2 in the outlet streams were monitored by gas chromatography with a HP-PLOT Q column from Agilent and a flame ionization detector with a methanator (hydrogenation reactor).

CeO_2 as Catalyst for Imine Synthesis

Calcined CeO_2 (50 mg) was added to a mixture of benzyl alcohol (10 mmoL) and aniline (20 mmoL). The resulting mixtures were stirred vigorously at 500 rpm at 50 °C. After a certain time (at least 3 h), the reaction mixtures were diluted with methanol (6 μL/mL), filtered and transferred to new vials. The imine product was analyzed using HPLC (Shimadzu LC-20AT, Japan) equipped with a Hypersil ODS C18 column (5 μm in a size of 4.6 mm × 250 mm), and the mobile phase was methanol : water = 8 : 2. To compare with the other reactions, reaction rates are given as the amount of imine formation per hour per catalyst mass (mmol h^{-1} g^{-1}).

Acknowledgements

This research was supported by National Natural Science Foundation of China (Grant number 21601121), the Program for Professor of Special Appointment (Eastern Scholar) at Shanghai Institutions of Higher Learning (Grant number QD2016037), and Young Professor Cultivation Program of Shanghai Municipal University (Grant number ZZGCD16019). G.R. acknowledge support by the Austrian Science Fund (FWF, DK + Solids4Fun) (Grant number W1243) and SUES for a "Renowned Overseas Professor" grant..

Conflict of Interest

The authors declare no conflict of interest.

Keywords: Catalyst · CeO_2 nanoflakes · CO oxidation · Imine synthesis · Lamellar structure

[1] a) L. Lukashuk, K. Foettinger, E. Kolar, C. Rameshan, D. Teschner, M. Haevecker, A. Knop-Gericke, N. Yigit, H. Li, E. McDermott, M. Stoeger-Pollach, G. Rupprechter, *J. Catal.* **2016**, *344*, 1–15; b) J. Yang, L. Lukashuk, J. Akbarzadeh, M. Stoeger-Pollach, H. Peterlik, K. Foettinger, G. Rupprechter, U. Schubert, *Chem. Eur. J.* **2015**, *21*, 885–892; c) J. Yang,

Table 2. Synthesis conditions of CeO_2 by the microwave-assisted solution method.

No.	*Sample*	*Conditions*					
		Microwave (MW)[a]	Ultrasonic (US)[b]	Ultraviolet (UV)[c]	Pressure (P)	Container	Temperature program
1	A (reference)	–	–	–	√[d]	Teflon inline	180 °C[e], 6 h
2	MW	√	–	–	–	Quartz flask	15 °C/min to 180 °C, then kept at 180 °C for 10 min
3	MW + P	√	–	–	√ (3 atm)	Teflon inline	
4	MW + US	√	√	–	–	Quartz flask	
5	MW + UV	√	–	√	–	Quartz flask	
6	MW + US + UV	√	√	√	–	Quartz flask	

[a] Microwave power adjusted in the range of 0–1000 W by variable frequency. [b] The powder of US was 300 W. [c] The wavelength of ultraviolet light was 365 nm and the powder was 300 W. [d] The Teflon inline was sealed in a steel autoclave, and kept still. [e] The autoclave was put in an oven with 180 °C.

© 2018 Wiley-VCH Verlag GmbH & Co. KGaA, Weinheim

L. Lukashuk, H. Li, K. Foettinger, G. Rupprechter, U. Schubert, *Catal. Lett.* **2014**, *144*, 403–412; d) X. Yu, X. Yang, G. Li, *J. Mater. Sci. Mater. Electron.* **2016**, *27*, 12174–12177.

[2] a) Y. E. Jeong, P. A. Kumar, H. P. Ha, K.-y. Lee, *Catal. Lett.* **2017**, *147*, 428–441; b) J. Xu, G. Lu, Y. Guo, Y. Guo, X.-Q. Gong, *Appl. Catal. A* **2017**, *535*, 1–8.

[3] a) M. Tamura, K. Tomishige, *Angew. Chem. Int. Ed.* **2015**, *54*, 864–867; *Angew. Chem.* **2015**, *127*, 878–881; b) L. Geng, J. Song, Y. Zhou, Y. Xie, J. Huang, W. Zhang, L. Peng, G. Liu, *Chem. Commun.* **2016**, *52*, 13495–13498; c) B. Govinda Rao, P. Sudarsanam, A. Rangaswamy, B. M. Reddy, *Catal. Lett.* **2015**, *145*, 1436–1445; d) P. Sudarsanam, B. Hillary, M. H. Amin, S. B. A. Hamid, S. K. Bhargava, *Appl. Catal. B: Environ.* **2016**, *185*, 213–224; e) J. Zhang, J. Yang, J. Wang, H. Ding, Q. Liu, U. Schubert, Y. Rui, J. Xu, *Molecular Catalysis* **2017**, *443*, 131–138; f) H. Zhang, C. Wu, W. Wang, J. Bu, F. Zhou, B. Zhang, Q. Zhang, *Appl. Catal. B* **2018**, *227*, 209–217.

[4] a) S. Phanichphant, A. Nakaruk, D. Channei, *Appl. Surf. Sci.* **2016**, *387*, 214–220; b) S. Kumar, A. K. Ojha, *RSC Adv.* **2016**, *6*, 8651–8660; c) A. Gogoi, M. Navgire, K. C. Sarma, P. Gogoi, *Chem. Eng. J.* **2017**, *311*, 153–162.

[5] a) M. M. Natile, G. Boccaletti, A. Glisenti, *Chem. Mater.* **2005**, *17*, 6272–6286; b) H. Wang, J.-J. Zhu, J.-M. Zhu, X.-H. Liao, S. Xu, T. Ding, H.-Y. Chen, *Phys. Chem. Chem. Phys.* **2002**, *4*, 3794–3799; c) R. C. Deus, C. R. Foschini, B. Spitova, F. Moura, E. Longo, A. Z. Simoes, *Ceram. Int.* **2014**, *40*, 1–9; d) R. C. Deus, M. Cilense, C. R. Foschini, M. A. Ramirez, E. Longo, A. Z. Simoes, *J. Alloys Compd.* **2013**, *550*, 245–251; e) C.-Y. Cao, Z.-M. Cui, C.-Q. Chen, W.-G. Song, W. Cai, *J. Phys. Chem. C* **2010**, *114*, 9865–9870.

[6] H. Liu, H. Liu, X. Han, *J. Solid State Electrochem.* **2017**, *21*, 291–295.

[7] a) A. Phuruangrat, T. Thongtem, S. Thongtem, *Mater. Lett.* **2017**, *193*, 161–164; b) O. S. Bezkrovnyi, R. Lisiecki, L. Kepinski, *Cryst. Res. Technol.* **2016**, *51*, 554–560; c) Y. Tao, F. H. Gong, H. Wang, H. P. Wu, G. L. Tao, *Mater. Chem. Phys.* **2008**, *112*, 973–976.

[8] A. Phuruangrat, S. Thongtem, T. Thongtem, *Mater. Lett.* **2017**, *196*, 61–63.

[9] S. Hilaire, L. Luo, F. Rechberger, F. Krumeich, M. Niederberger, *Z. Anorg. Allg. Chem.* **2014**, *640*, 733–737.

[10] A. Umar, R. Kumar, M. S. Akhtar, G. Kumar, S. H. Kim, *J. Colloid Interface Sci.* **2015**, *454*, 61–68.

[11] a) S. Bensaid, N. Russo, D. Fino, *Catal. Today* **2013**, *216*, 57–63; b) S. Premlatha, P. Sivasakthi, G. N. K. Ramesh Bapu, *J. Electroanal. Chem.* **2017**, *788*, 107–117.

[12] a) R.-R. Cui, W.-C. Lu, L.-M. Zhang, B.-H. Yue, S.-S. Shen, *J. Phys. Chem. C* **2009**, *113*, 21520–21525; b) P. Xu, H. Niu, J. Chen, J. Song, C. Mao, S. Zhang, Y. Gao, C. Chen, *J. Nanopart. Res.* **2016**, *18*, 1–9.

[13] a) J. Cui, J. Luo, B. Peng, X. Zhang, Y. Zhang, Y. Wang, Y. Qin, H. Zheng, X. Shu, Y. Wu, *Nanoscale* **2016**, *8*, 770–774; b) N. K. Eswar, V. V. Katkar, P. C. Ramamurthy, G. Madras, *Ind. Eng. Chem. Res.* **2015**, *54*, 8031–8042.

[14] a) H. Huang, J. Huang, W. Liu, Y. Fang, Y. Liu, *ACS Appl. Mater. Interfaces* **2017**, *9*, 39380–39390; b) D.-W. Lee, M.-H. Jin, D. Oh, S.-W. Lee, J.-S. Park, *ACS Sustainable Chem. Eng.* **2017**, *5*, 9935–9944; c) Z. Qiu, Y. Ma, K. Edstroem, G. A. Niklasson, T. Edvinsson, *Int. J. Hydrogen Energy* **2017**, *42*, 28397–28407; d) M. Zhu, Y. Osakada, S. Kim, M. Fujitsuka, T. Majima, *Appl. Catal. B* **2017**, *217*, 285–292; e) X. Li, Z. Liu, L. Song, D. Wang, Z. Zhang, *Electrochim. Acta* **2018**, *263*, 561–569; f) B. Zhang, Y. H. Lui, A. P. S. Gaur, B. Chen, X. Tang, Z. Qi, S. Hu, *ACS Appl. Mater. Interfaces* **2018**, *10*, 8739–8748.

[15] X. Chen, X. Chen, E. Yu, S. Cai, H. Jia, J. Chen, P. Liang, *Chem. Eng. J. (Amsterdam, Neth.)* **2018**, *344*, 469–479.

[16] P. S. Barbato, S. Colussi, A. Di Benedetto, G. Landi, L. Lisi, J. Llorca, A. Trovarelli, *J. Phys. Chem. C* **2016**, *120*, 13039–13048.

[17] W. Zhu, S. Xiao, D. Zhang, P. Liu, H. Zhou, W. Dai, F. Liu, H. Li, *Langmuir* **2015**, *31*, 10822–10830.

[18] a) A. M. Duarte de Farias, D. Nguyen-Thanh, M. A. Fraga, *Appl. Catal. B* **2010**, *93*, 250–258; b) Y. Lee, G. He, A. J. Akey, R. Si, M. Flytzani-Stephanopoulos, I. P. Herman, *J. Am. Chem. Soc.* **2011**, *133*, 12952–12955.

[19] X. Zhang, F. Hou, Y. Yang, Y. Wang, N. Liu, D. Chen, Y. Yang, *Appl. Surf. Sci.* **2017**, *423*, 771–779.

[20] Z. Wu, M. Li, S. H. Overbury, *J. Catal.* **2012**, *285*, 61–73.

[21] C. Schilling, A. Hofmann, C. Hess, M. V. Ganduglia-Pirovano, *J. Phys. Chem. C* **2017**, *121*, 20834–20849.

[22] a) M. G. Sanchez, J. L. Gazquez, *J. Catal.* **1987**, *104*, 120–135; b) J. Lee, Y. Ryou, X. Chan, T. J. Kim, D. H. Kim, *J. Phys. Chem. C* **2016**, *120*, 25870–25879.

[23] a) M. Yin, W. Qiu, L. Song, H. Zhu, Y. Chen, S. Li, J. Cheng, Y. Sun, G. Bai, G. Zhang, H. He, *ChemistrySelect* **2018**, *3*, 2683–2691; b) S. Damyanova, C. A. Perez, M. Schmal, J. M. C. Bueno, *Appl. Catal. A* **2002**, *234*, 271–282; c) K. Cheng, W. Song, Y. Cheng, J. Liu, Z. Zhao, Y. Wei, *Catal. Sci. Technol.* **2016**, *6*, 4478–4490.

[24] a) H.-H. Liu, Y. Wang, A.-P. Jia, S.-Y. Wang, M.-F. Luo, J.-Q. Lu, *Appl. Surf. Sci.* **2014**, *314*, 725–734; b) M.-F. Luo, J.-M. Ma, J.-Q. Lu, Y.-P. Song, Y.-J. Wang, *J. Catal.* **2007**, *246*, 52–59; c) M. Han, X. Wang, Y. Shen, C. Tang, G. Li, R. L. Smith, Jr., *J. Phys. Chem. C* **2010**, *114*, 793–798.

[25] a) Z. Zhang, Y. Wang, J. Lu, J. Zhang, M. Li, X. Liu, F. Wang, *ACS Catal.* **2018**, *8*, 2635–2644; b) J. M. López, A. L. Gilbank, T. García, B. Solsona, S. Agouram, L. Torrente-Murciano, *Appl. Catal. B* **2015**, *174*, 403–412.

Manuscript received: May 14, 2018
Accepted Article published: July 11, 2018
Version of record online: ■■, ■■■■

© 2018 Wiley-VCH Verlag GmbH & Co. KGaA, Weinheim

FULL PAPERS

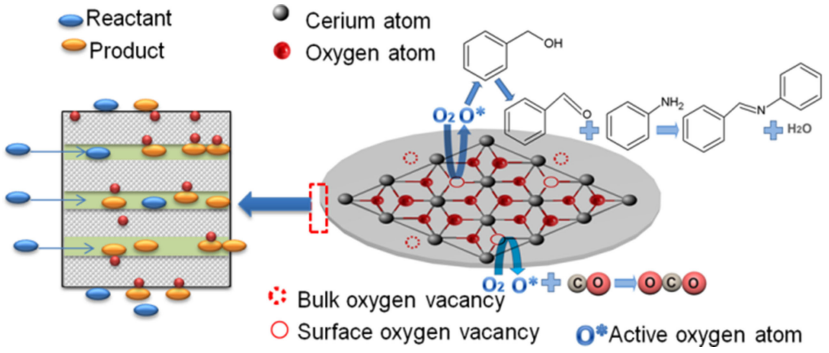

CeO promotion: CeO_2 nanoflakes obtained by microwave-assisted synthesis were composed of 5–6 nm nanoparticles, laminated with 3.42–3.85 nm channel gaps. MW-assisting was beneficial toform a higher surface $Ce^{3+}/(Ce^{3+}+Ce^{4+})$ ratio and surface oxygen vacancies during short synthesis procedure. They were profitable to the excellent catalytic performance.

H. Ding, Dr. J. Yang, S. Ma, N. Yigit, Prof. J. Xu, Prof. G. Rupprechter, Dr. J. Wang**

1 – 10

Large Dimensional CeO_2 Nanoflakes by Microwave-Assisted Synthesis: Lamellar Nanochannels and Surface Oxygen Vacancies Promote Catalytic Activity